Adsorption Dynamics of Gases and Vapors on the Nanoporous Metal Organic Framework Material Ni 2 (4,4‘−Bipyridine) 3 (NO 3) 4 : Guest Modification of Host Sorption Behavior

ARTICLE *in* JOURNAL OF THE AMERICAN CHEMICAL SOCIETY · NOVEMBER 2001

Impact Factor: 12.11 · DOI: 10.1021/ja0109895 · Source: PubMed

Adsorption Dynamics of Gases and Vapors on the Nanoporous Metal Organic Framework Material $Ni_2(4,4'\text{-Bipyridine})_3(NO_3)_4$: Guest Modification of Host Sorption Behavior

Ashleigh J. Fletcher,[§] Edmund J. Cussen,[†] Timothy J. Prior,[†] Matthew J. Rosseinsky,[†] Cameron J. Kepert,[‡] and K. Mark Thomas*[,§]

Contribution from the Northern Carbon Research Laboratories, Department of Chemistry, Bedson Building, University of Newcastle upon Tyne, Newcastle upon Tyne, NE1 7RU, U.K., Department of Chemistry, University of Liverpool, Liverpool, L69 7ZD, U.K., and School of Chemistry, University of Sydney, New South Wales 2006, Australia

Received April 18, 2001

Abstract: This study combines measurements of the thermodynamics and kinetics of guest sorption with powder X-ray diffraction measurements of the nanoporous metal organic framework adsorbent (host) at different adsorptive (guest) loadings. The adsorption characteristics of nitrogen, argon, carbon dioxide, nitrous oxide and ethanol and methanol vapors on $Ni_2(4,4'\text{-bipyridine})_3(NO_3)_4$ were studied over a range of temperatures as a function of pressure. Isotherm steps were observed for both carbon dioxide and nitrous oxide adsorption at ∼10−20% of the total pore volume and at ∼70% of total pore volume for methanol adsorption. The adsorption kinetics obey a linear driving force (LDF) mass transfer model for adsorption at low surface coverage. At high surface coverage, both methanol and ethanol adsorption follow a combined barrier resistance/diffusion model. The rates of adsorption in the region of both the carbon dioxide and methanol isotherm steps were significantly slower than those observed either before or after the step. X-ray diffraction studies at various methanol loadings showed that the host structure disordered initially but underwent a structural change in the region of the isotherm step. These isotherm steps are ascribed to discrete structural changes in the host adsorbent that are induced by adsorption on different sites. Isotherm steps were not observed for ethanol adsorption, which followed a Langmuir isotherm. Previous X-ray crystallography studies have shown that all the sites are equivalent for ethanol adsorption on $Ni_2(4,4'\text{-bipyridine})_3(NO_3)_4$, with the host structure undergoing a scissoring motion and the space group remaining unchanged during adsorption. The activation energies and preexponential factors for methanol and ethanol adsorption were calculated for each pressure increment at which the linear driving force model was obeyed. There was a good correlation between activation energy and ln(preexponential factor), indicating a compensation effect. The results are discussed in terms of reversible adsorbate/adsorbent (guest/host) structural changes and interactions and the adsorption mechanism. The paper contains the first evidence of specific interactions between guests and functional groups leading to structural change in flexible porous coordination polymer frameworks.

Introduction

Adsorbents have many important applications, including their use in catalysis or as catalyst supports, in gas separation and purification, and in environmental protection through pollution control and abatement.[1−3] Some adsorbents with well-established applications, such as active carbons, are amorphous materials, and their pore structures may include a wide pore-size distribution, making them difficult to characterize. However, there is considerable interest in adsorbents that have a well-defined crystalline structure, for example, aluiminosilicates (zeolites) and aluminophosphates. Recently, crystalline porous materials based on metal-organic systems have been prepared in which the coordination polymer framework remains intact after removal of the solvent template/guest. These materials offer the possibility of designing and tailoring materials with well-defined pore size and shape for specific applications.

A number of highly porous and stable metal-organic framework materials have been prepared[3−18] on the basis of multidentate ligands whose geometry controls that of the network.

* To whom correspondence should be addressed. E-mail: mark.thomas@ncl.ac.uk.

† University of Liverpool.

‡ University of Sydney.

§ University of Newcastle upon Tyne.

(1) Rouquerol, F.; Rouquerol, J.; Sing, K. *Adsorption by Powders and Porous Solids*; Academic Press: London 1999.

(2) Barton, T. J.; Bull, L. M.; Klemperer, W. G.; Loy, D. A.; McEnaney, B.; Misono, M.; Monson, P. A.; Pez, G.; Scherer, G. W.; Vartuli, J. C.; Yaghi, O. M. *Chem. Mater.* **1999**, *11*, 2633.

(3) Yaghi, O. M.; Li, H.; Davis, C.; Richardson, D.; Groy, T. L. *Acc. Chem. Res.* **1998**, *31*, 474.

(4) Eddaoudi, M.; Li, H.; Yaghi, O. M. *J. Am. Chem. Soc.* **2000**, *122*, 1391.

(5) Reineke, T. M.; Eddaoudi, M.; Fehr, M.; Kelley, D.; Yaghi, O. M. *J. Am. Chem. Soc.* **1999**, *121*, 1651.

(6) Reineke, T. M.; Eddaoudi, M.; Moler, D.; O'Keeffe, M.; Yaghi, O. M. *J. Am. Chem. Soc.* **2000**, *122*, 4843.

(7) Hoskins, B. F.; Robson, R. *J. Am. Chem. Soc.***1990**, *112*, 1546.

(8) Endo, K.; Koike, T.; Sawaki, T.; Hayashida, O.; Masuda, H.; Aoyama, Y. *J. Am. Chem. Soc.* **1997**, *119*, 4117.

(9) Kondo, M.; Yoshitomi, T.; Seki, K.; Matsuzaka, H.; Kitagawa, S. *Angew. Chem., Int. Ed. Engl.* **1997**, *36*, 1725.

(10) Venkataraman, D.; Gardner, G. B.; Lee, S.; Moore, J. S. *J. Am. Chem. Soc.* **1995**, *117*, 11600.

(11) Zaworotko, M. J. *Chem. Commun.* **2001**, *1*, 1.

10.1021/ja0109895 CCC: $20.00
Published on Web 09/21/2001

The design of guest-specific frameworks requires a detailed understanding of the sorption behavior of this class of crystalline nanoporous materials, and a limited number of studies of gas and vapor sorption on metal-organic framework materials have been reported.[6,19−21] There are indications of the complex nature of the sorption process, especially in the cases in which coordination may change, distortion of the host structure may occur to accommodate adsorbate (guest) molecules, and framework structural integrity may be compromised. At low temperature, there is the added complication of activated diffusion effects in the adsorption process. There has been the suggestion that a pore-blocking process may take place on the basis of isotherm shapes at low relative pressure.[20]

$Ni_2(4,4'\text{-bipyridine})_3(NO_3)_4$ is a porous framework material that is capable of undergoing reversible guest exchange. This material has been shown by X-ray crystallographic studies to desorb two molecules of ethanol per $Ni_2(4,4'\text{-bipyridine})_3(NO_3)_4$ unit with a small change in structure involving a scissors movement in which two cell dimensions increase while the other decreases, with the space group (*Ccca*) remaining unchanged.[22] The pores are composed of channels of cavities of 360 × 760 pm linked by windows of 232 × 275 pm (based on calculations using van der Waals radii) between adjacent bipyridine ligands parallel to the *a* axis. The ethanol molecule forms a hydrogen bond to one nitrate coordinated to the nickel. This study provided direct proof of a subtle structural change between the completely desolvated and the fully solvated states,[22] but there have also been studies[10,23] of cell dimension changes in partially desolvated systems without structural analysis. Salts are also formed with chlorobenzene, *o*-dichlorobenzene, benzene, nitrobenzene, toluene or anisole,[24] carbon disulfide, and water.[9,25] It is apparent that the metal-organic framework material $Ni_2(4,4'\text{-bipyridine})_3(NO_3)_4$, has a well-defined pore size and shape and is capable of adsorbing a wide range of adsorptives ranging from nonpolar to hydrophilic adsorptives. In other similar materials, the removal of the solvent may lead to symmetry changes[26] or pore volume collapse.[21]

The uniformity of the pore structure in $Ni_2(4,4'\text{-bipyridine})_3(NO_3)_4$, coupled with the knowledge that the adsorbent structure changes when the pores are filled with ethanol, allows the possibility of studying the dynamic processes by which the adsorbate (guest) and adsorbent (host) structure may change under the influence of the adsorption process. In this study, the adsorption characteristics of a series of gases and vapors on $Ni_2(4,4'\text{-bipyridine})_3(NO_3)_4$ have been investigated in detail to establish the influence of adsorbate structural factors on adsorption characteristics. These studies have been combined with X-ray diffraction studies of host/guest structure at various stages of pore filling to establish structural changes during the adsorption process. The specific chemistry arising from the interaction of different guests with the functionalized pores is often advanced as a reason for studying metal-organic framework materials. Here, we show that the structure and functional group character of the guest produces distinct features in both the kinetics and thermodynamics of sorption by the coordination polymer framework, with its well-defined array of functionalized sorption sites.

Experimental Section

Materials Used. The porous framework material used in this study was prepared as described previously.[22] The gases used were supplied by BOC Ltd, London, U.K. and had the following purities: carbon dioxide, 99.999%; nitrous oxide, 99.997%; nitrogen, 99.999%; and argon, 99.99%. Methanol (99.9%) and ethanol (99.9%) were obtained from Aldrich Chemicals, U.K.

Measurement of Adsorption Kinetics. The adsorption isotherm and kinetic measurements were carried out using an Intelligent Gravimetric Analyzer (IGA) supplied by Hiden Analytical Ltd, Warrington, U.K.[27] The instrument is an ultrahigh vacuum system with a fully computerized microbalance, which allows adsorption/desorption isotherms and the corresponding kinetics for each pressure increment to be determined, with the approach to equilibrium being monitored in real time using a computer algorithm.[28−34] The condition for achieving equilibrium was 99.9% of the predicted value calculated in real time by fitting the uptake profile to an exponential kinetic decay model. The balance and pressure control systems were fully thermostated to 0.2 K to eliminate the effects of changes in the external environment. The microbalance had a long-term stability of ±1 μg with a weighing resolution of 0.2 μg. The adsorbent sample (∼100 mg) was outgassed to a constant weight at 353 K and 10^{-5} Pa prior to measurement of the isotherms. The pressure was monitored by three pressure transducers with ranges of 0−0.2 kPa, 0−10 kPa, and 0−1 MPa. The liquid used to generate the vapor was degassed fully by repeated evacuation and vapor equilibration cycles of the liquid supply side of the vapor reservoir. The vapor pressure was gradually increased, over a time-scale of ∼30 s to prevent disruption of the microbalance, until the desired value was achieved. Therefore, the period over which the pressure change occurred was very small when compared with the adsorption kinetics. The accuracy of the set-point pressure regulation was ±0.02% of the range used. The pressure was maintained at the set point by active computer control of inlet/outlet valves throughout the duration of the adsorption kinetic experiments. The sample temperature was measured at ∼5 mm from the sample and was controlled to ±0.05 K throughout the duration of the experiment by circulation of a 1:1 mixture of ethylene glycol and water from a computer-controlled water bath. The initial pressure increment from high vacuum ($<10^{-5}$ Pa) resulted in a change of temperature of ∼0.5 K because of the introduction of conduction from the thermostatically controlled water jacket through the gas to the sample. The isotherms were typically repeatable to better than ±1%.

The saturated vapor pressures were calculated using the following equation[35,36]

(12) Li, H.; Laine, A.; O'Keeffe, M.; Yaghi, O. M. *Science* **1999**, *283* (5405), 1145.
(13) Gardner, G. B.; Venkataraman, D.; Moore, J. S.; Lee, S. *Nature* **1995**, *374*, 792.
(14) Li, H.; Eddaoudi, M.; Groy, T. L.; Yaghi, O. M. *J. Am. Chem. Soc.* **1998**, *120*, 8571.
(15) Yaghi, O. M.; Li, H.; Groy, T. L. *Inorg. Chem.* **1997**, *36*, 4292.
(16) Seo, J. S.; Whang, D.; Lee, H.; Jun, S. I.; Oh, J.; Jeon, Y. J.; Kim, K. *Nature* **2000**, *404* (6781), 982.
(17) Eddaoudi, M.; Moler, D. B.; Li, H.; Chen, B.; Reineke, T. M.; O'Keeffe, M.; Yaghi, O. M. *Acc. Chem. Res.* **2001**, *34*, 319.
(18) Kepert, C. J.; Prior, T. J.; Rosseinsky, M. J. *J. Am. Chem. Soc.* **2000**, *122*, 5158.
(19) Kondo, M.; Shimamura, M.; Noro, S.; Minakoshi, S.; Asami, A.; Seki, K.; Kitagawa, S. *Chem. Mater.* **2000**, *12*, 1288.
(20) Li, D.; Kaneko, K. *J. Phys. Chem. B* **2000**, *104*, 8940.
(21) Li, D.; Kaneko, K. *Chem. Phys. Lett.* **2001**, *335*, 50.
(22) Kepert, C. J.; Rosseinsky, M. J. *Chem. Commun.***1999**, 375.
(23) Brunet, P.; Simard, M.; Wuest, J. D. *J. Am. Chem. Soc.* **1997**, *119*, 2737.
(24) Biradha, K.; Mondal, A.; Moulton, B.; Zaworotko, M. J. *Dalton* **2000**, *21*, 3837.
(25) Power, K. N.; Hennigar, T. L.; Zaworotko, M. J. *New J. Chem.* **1998**, *22*, 177.
(26) Kepert, C. J.; Hesek, D.; Beer, P. D.; Rosseinsky, M. J. *Angew. Chem., Int. Ed. Engl.* **1998**, *37*, 3158.
(27) Benham, M. J.; Ross, D. K. *Z. Phys. Chem.* **1989**, *163*, 25.
(28) Reid, C. R.; O'koye, I. P.; Thomas, K. M. *Langmuir* **1998**, *14*, 2415.
(29) Reid, C. R.; Thomas, K. M. *Langmuir* **1999**, *15*, 3206.
(30) Harding, A. W.; Foley, N. J.; Norman, P. R.; Francis, D. C.; Thomas, K. M. *Langmuir* **1998**, *14*, 3858.
(31) O'koye, I. P.; Benham, M.; Thomas, K. M. *Langmuir* **1997**, *13*, 4054.
(32) Foley, N. J.; Forshaw, P. L.; Thomas, K. M.; Stanton, D.; Norman, P. R. *Langmuir* **1997**, *13*, 2083.
(33) Fletcher, A. J.; Thomas, K. M. *Langmuir* **1999**, *15*, 6908.
(34) Fletcher, A. J.; Thomas, K. M. *Langmuir* **2000**, *16*, 6253.
(35) *Lange's Handbook of Chemistry*, 15th ed.; McGraw-Hill: New York, 1999.

$$\log_{10} p = A - \frac{B}{T + C} \quad (1)$$

where p is the saturated vapor pressure (Torr), T is the temperature in degrees Celsius, and A, B, and C are constants defined by the adsorbate. Methanol: $A = 7.89750$, $B = 1474.08$, $C = 229.13$; ethanol: $A = 8.32109$, $B = 1718.10$, $C = 237.52$; carbon dioxide: $A = 7.810237$, $B = 995.7048$, $C = 293.4754$; nitrous oxide: $A = 7.00394$, $B = 654.260$, $C = 247.16$.

X-ray Diffraction Measurements. X-ray diffraction experiments were performed on samples of partially loaded porous framework material contained in sealed Lindemann capillaries. The samples were prepared by outgassing at 10^{-1} Pa and 353 K for 24 h, followed by loading the material with methanol vapor at 300 K and pressures $p/p^0 = 0.044$, 0.326, 0.673, and 0.973 corresponding to 50, 75, 87.5, and ~100% loading, respectively. Data were also collected from an evacuated sample in order to determine the effect of this process on the crystallinity. Powder diffraction data were recorded in the angular range $5 \leq 2\theta \leq 30°$ on a Stoe Stadi-P diffractometer with a linear position-sensitive detector and monochromatic Cu $K_{\alpha 1}$ radiation from a germanium monochromator.

Results

Adsorption Isotherms. In this paper, the term pressure increment is used to describe pressure changes used to generate the isotherm, whereas isotherm steps refer to changes in isotherm shape. Adsorption isotherms for nitrogen and argon on $Ni_2(4,4'\text{-bipyridine})_3(NO_3)_4$ at 273K are shown in Figure 1a. It is apparent that the argon isotherm is very close to linearity up to 100 kPa, but the nitrogen isotherm shows some curvature at low pressure. Studies of nitrogen adsorption at 77 K showed that nitrogen was not adsorbed under these conditions. This is presumably because of activated diffusion effects associated with the low thermal energy of the adsorbate relative to the high barrier for diffusion through the barriers with dimensions of 232 × 275 pm (based on calculations using van der Waals radii) formed between adjacent 4,4′-bipyridine molecules. The adsorption isotherm for nitrous oxide at 273 K and carbon dioxide in the temperature range 268−303 K are shown in Figures 1b and c, respectively. Comparison of the nitrous oxide and carbon dioxide adsorption isotherms shows that there are steps in the isotherms at similar relative pressures (CO_2, $p/p^0 \sim 0.001-0.002$; N_2O, $p/p^0 \sim 0.0013$). The hysteresis in the adsorption/desorption isotherms at 273 K was very small. Closer inspection of the isotherm also shows a much smaller, barely distinguishable, step at $p/p^0 \sim 3 \times 10^{-4}$. However, the carbon dioxide adsorption isotherm at 303 K does not show a well-defined step, although the isotherm has curvature, which is possibly a vestigial part of the step observed at lower temperature.

The methanol (273−293 K) and ethanol (293−323 K) isotherms are shown in Figure 1d and e, respectively. It is apparent that the ethanol adsorption isotherm is type I in the IUPAC classification scheme.[1] However, all of the methanol isotherms have a step in the isotherm at ~70% of the total pore volume (loading), depending on the temperature. The total pore volumes obtained from the methanol and ethanol adsorption isotherms were ~0.148 and ~0.149 $cm^3\ g^{-1}$, respectively. The total pore volume calculated from the stoichiometry determined using crystallographic data for $Ni_2(4,4'\text{-bipyridine})_3(NO_3)_4 \cdot 2C_2H_5OH$ was 0.142 $cm^3\ g^{-1}$. The uptake's being slightly larger (4−5%) than the stoichiometry obtained from the X-ray crystallographic studies may be ascribed to defects in the structure of the material. The stoichiometries estimated at $p/p^0 = 1$ were $Ni_2(4,4'\text{-bipyridine})_3(NO_3)_4 \cdot 2.13C_2H_5OH$ and $Ni_2(4,4'\text{-bipyridine})_3(NO_3)_4 \cdot 3.05CH_3OH$.

Adsorption Kinetics. Linear driving force (LDF),[28−34] a combined barrier resistance/Fickian diffusion[28,29,33,34,37] and Fickian models[29,38] provide satisfactory descriptions in most cases of the adsorption kinetics of various gases/vapors on carbon molecular sieves and active carbons, depending on the adsorptive and experimental conditions. The LDF model is described by eq 2,

$$M_t/M_e = 1 - \exp(-kt) \quad (2)$$

where M_t is the mass uptake at time t, M_e is the mass uptake at equilibrium, and k is the kinetic rate constant. The adsorption kinetics can be compared in terms of the rate constant (k) for the LDF model, which can be determined from either the gradient of the $\ln(1 - M_t/M_e)$ against time plot or by fitting the adsorption uptake curves to eq 2. Graphs of M_t/M_e versus time for typical adsorption increments for methanol and ethanol adsorption are provided in Supporting Information, together with the corresponding fit for the LDF model. The kinetic data obtained from the LDF model for methanol and ethanol adsorption are also given in Supporting Information. Figure 2 shows the variation of rate constant with amount adsorbed for ethanol adsorption (298 K) and methanol adsorption (273 K). It is apparent that the rate constant decreases with increasing relative pressure and increasing surface coverage for ethanol reaching a minimum before increasing with further increase in surface coverage. A similar trend is observed for all of the temperatures studied. The kinetic measurements for the first adsorption pressure increment are subject to larger uncertainty than the other kinetic measurements, because there is a change from ultrahigh vacuum under outgas conditions to a vapor pressure, which introduces conduction through the gas, resulting in larger temperature fluctuations at the start of the pressure increment. In the case of methanol, the changes in the rate constants with relative pressure are small and tend to decrease with increasing surface coverage (loading), as shown in Figure 2.

Methanol adsorption deviates from the LDF model at $p/p^0 > 0.048$ (uptake, ~2 $mmol g^{-1}$ or ~50% of total pore volume), while ethanol deviates at $p/p^0 > 0.078$ (uptake, ~2.3 $mmol g^{-1}$ or ~ 90% of total pore volume). Therefore, another model is required to describe the adsorption kinetics in these cases.

A combined barrier resistance/diffusion (CBRD) model[37] is based on the existence of a barrier resistance at the surface and subsequent diffusion in a spherical microporous system by Fick's law.[38] The relevant equations for isothermal diffusion into a spherical particle with this model are as follows:

$$\frac{\partial C}{\partial t} = D\left(\frac{\partial^2 C}{\partial r^2}\right) + \left(\frac{2}{r}\right)\left(\frac{\partial C}{\partial r}\right) \quad (3)$$

where D is the crystallite diffusivity ($cm^2\ s^{-1}$), C is the sorbate concentration in the crystallite ($mmol\ cm^{-3}$), r is the radial coordinate, and t is the time.

$$D\frac{\partial C(r_c,t)}{\partial r} = k_b\{C^*(t) - C(r,t)\} \quad (4)$$

where D is the crystallite diffusivity ($cm^2\ s^{-1}$), k_b is the barrier

(36) CRC *Handbook of Chemistry and Physics*, 74th ed.; CRC Press: Boca Ratan, FL; 1993.

(37) Loughlin, K. F.; Hassan, M. M.; Fatehi, A. I.; Zahur, M. *Gas Sep. Purif.* **1993**, *7*, 264.

(38) Crank, J. *The Mathematics of Diffusion*, 2nd ed.; Clarendon Press: Oxford, 1975.

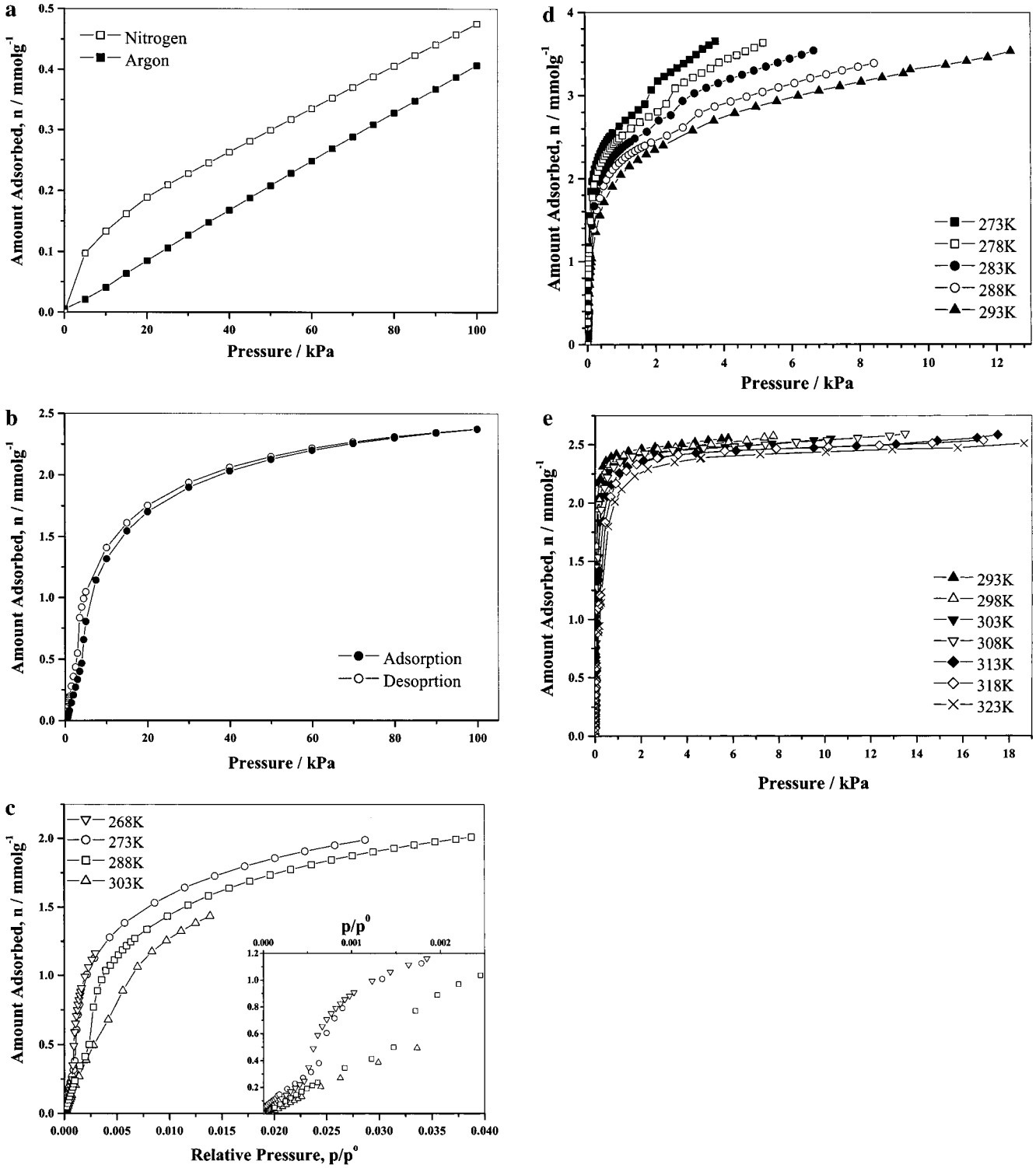

Figure 1. (a) Adsorption isotherms for nitrogen and argon on $Ni_2(4,4'\text{-bipyridine})_3(NO_3)_4$ at 273 K. (b) Adsorption/desorption isotherms for nitrous oxide $Ni_2(4,4'\text{-bipyridine})_3(NO_3)_4$ at 273 K. (c) Adsorption isotherms for carbon dioxide on $Ni_2(4,4'\text{-bipyridine})_3(NO_3)_4$ in the temperature range 268−303 K and pressure range p/p^0, 0−0.04 (p/p^0, 0−0.0025, inset). (d) Adsorption isotherms for methanol on $Ni_2(4,4'\text{-bipyridine})_3(NO_3)_4$ in the temperature range 273−293 K. (e) Adsorption isotherms for ethanol on $Ni_2(4,4'\text{-bipyridine})_3(NO_3)_4$ in the temperature range 293−323 K.

resistance (cm s^{-1}), r is the radial coordinate, r_c is the radius of the crystallite (cm), t is time, C is the sorbate concentration in the crystallite (mmol cm^{-3}), and C^* is the surface concentration in equilibrium with the gas phase (mmol cm^{-3}). The parameters derived from the model are k_b, the barrier resistance constant, and k_d, which is equal to D/r_c^2. A full description of the method used for solving the equation has been described previously.[29]

A comparison of the calculated profile from the combined barrier resistance/diffusion model with the experimental profile for typical pressure increments for methanol adsorption at 273 K is shown in Figure 3. The isotherm point in the Figure refers to the kinetics in going from the previous point to the equilibrium point. It is apparent that the CBRD model provides a good description of the adsorption kinetics for those pressure

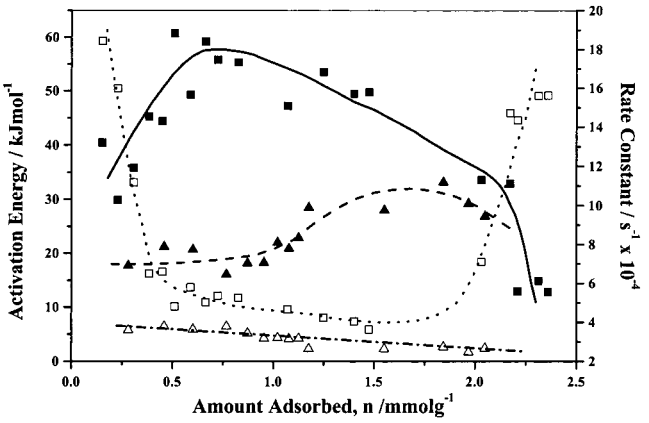

Figure 2. The variation of rate constant (open symbols) and activation energy (solid symbols) with amount adsorbed for adsorption of methanol (▲(273−293 K), △273 K) and ethanol (■(293−323K), □298 K) on $Ni_2(4,4'\text{-bipyridine})_3(NO_3)_4$.

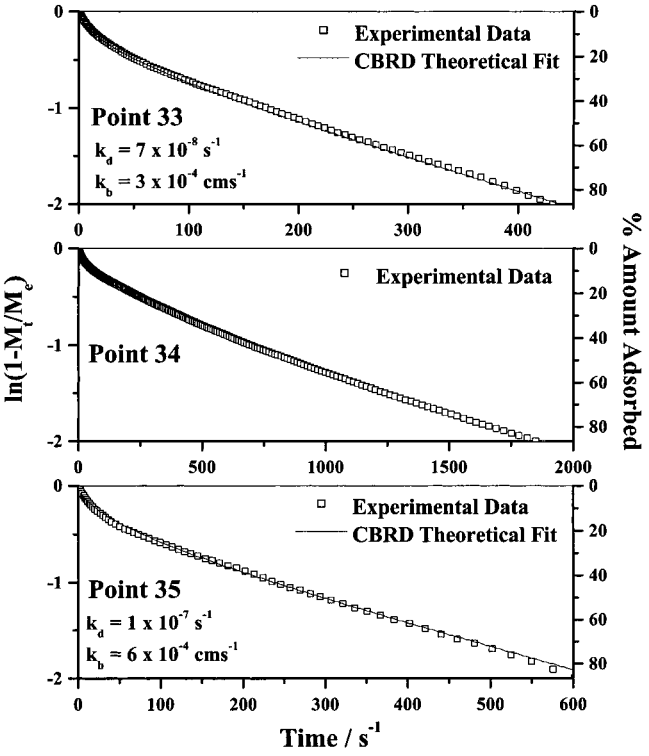

Figure 3. Comparison of the calculated profiles for the $\ln(1 - M_t/M_e)$ versus time graphs from the combined barrier resistance/diffusion model with the experimental profile for pressure increments in the region of the isotherm step for methanol adsorption on $Ni_2(4,4'\text{-bipyridine})_3(NO_3)_4$ at 273 K.

increments both before and after the step in the isotherm (isotherm point 34 in Figure 3) but not for the kinetics associated with the step itself. Additional data for adsorption at 278 K are provided in Supporting Information. Both the linear driving force and the combined barrier resistance/diffusion models give $\ln(1 - M_t/M_e)$ against time graphs that are linear above $M_t/M_e > 0.6$, ($\ln(1 - M_t/M_e) = -1$), and therefore, curvature in the graphs above this value is indicative of the data not fitting either model. Kinetic parameters obtained from the CBRD model for isotherm points prior to and after the isotherm step at 273 and 278 K are given in Table 1. It can be shown qualitatively from the vapor uptake versus time curves and the time required to reach equilibrium that the adsorption kinetics associated with the isotherm step are significantly slower, although still smooth. It

Table 1. Kinetic Data for Methanol Adsorption on $Ni_2(4,4'\text{-bipyridine})_3(NO_3)_4$ in the Region of the Step in the Isotherm Obtained from the Combined Barrier-Resistance/Diffusion Model

temp K	step	p/p^o	diff. coeff k_d/s^{-1}	barrier−resistance const k_b cm s^{-1}
273	32	0.2910−0.3366	1.00×10^{-7}	3.00×10^{-4}
	33	0.3366−0.3847	7.00×10^{-8}	3.00×10^{-4}
	34	0.3847−0.4323		
	35	0.4323−0.4798	1.00×10^{-7}	6.00×10^{-4}
	36	0.4798−0.5295	8.00×10^{-8}	5.00×10^{-3}
278	31	0.2399−0.2910	1.70×10^{-7}	2.50×10^{-4}
	32	0.2910−0.3366	1.15×10^{-7}	5.00×10^{-3}
	33	0.3366−0.3847		
	34	0.3847−0.4323	1.20×10^{-7}	2.50×10^{-4}
	35	0.4323−0.4798	7.00×10^{-8}	5.00×10^{-3}

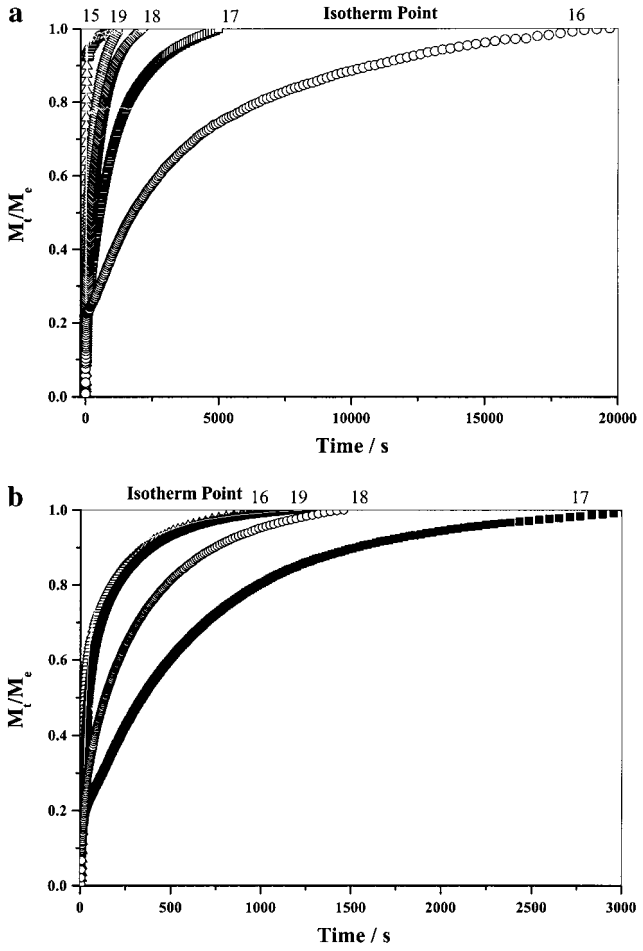

Figure 4. Comparison of gas adsorption kinetic profiles for M_t/M_e versus time for adsorption of gases on $Ni_2(4,4'\text{-bipyridine})_3(NO_3)_4$ in the region of the isotherm steps (a) carbon dioxide, (b) nitrous oxide.

is apparent that the isotherm steps in both methanol adsorption isotherms at 273 and 278 K are associated with changes in kinetic mechanism. Neither the LDF nor CBRD models work for the isotherm point associated with the isotherm step.

The adsorption of both carbon dioxide and nitrous oxide also have steps in the isotherms. In both cases, the adsorption kinetics for the isotherm step are also much slower than either before or after the isotherm step, as shown in the graphs of M_t/M_e (fractional uptake for the pressure increment) versus time (Figure 4). These profiles are characterized by a rapid uptake of 0.2−0.25 of the total uptake for the pressure increment followed by a slow uptake. The slow uptake region has a linear graph of

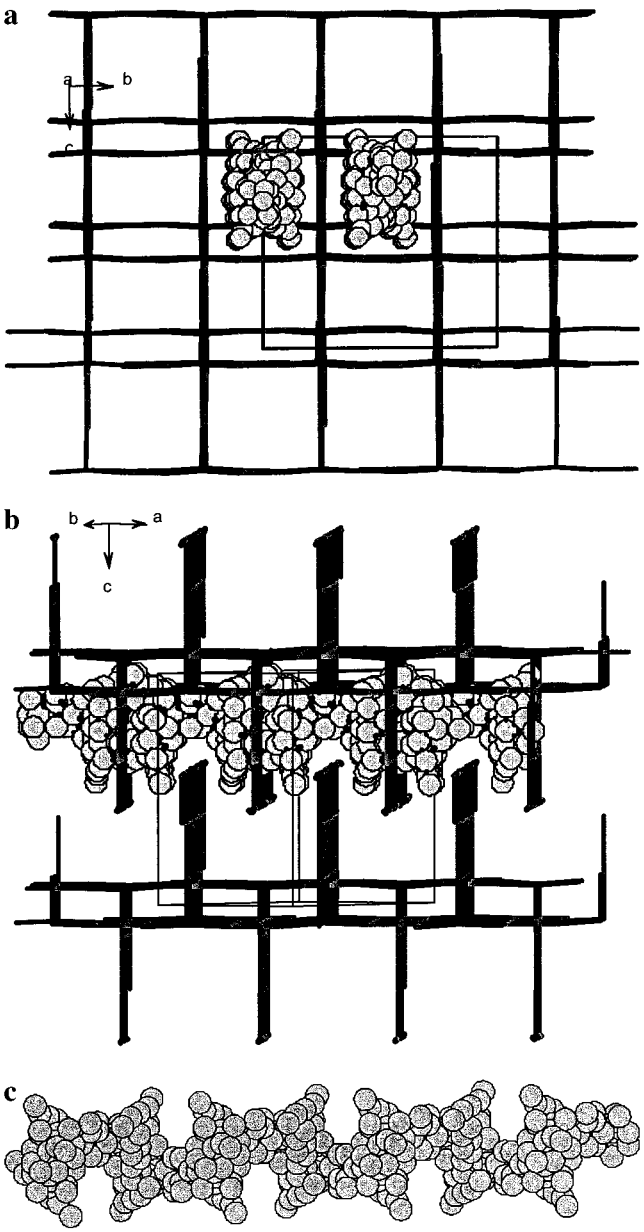

Figure 5. Structural characteristics of methanol adsorbed on Ni_2(4,4′-bipyridine)$_3(NO_3)_4$ (a) along *a* axis direction, (b) showing packing in the pores, and (c) the adsorbed ethanol in the pores.

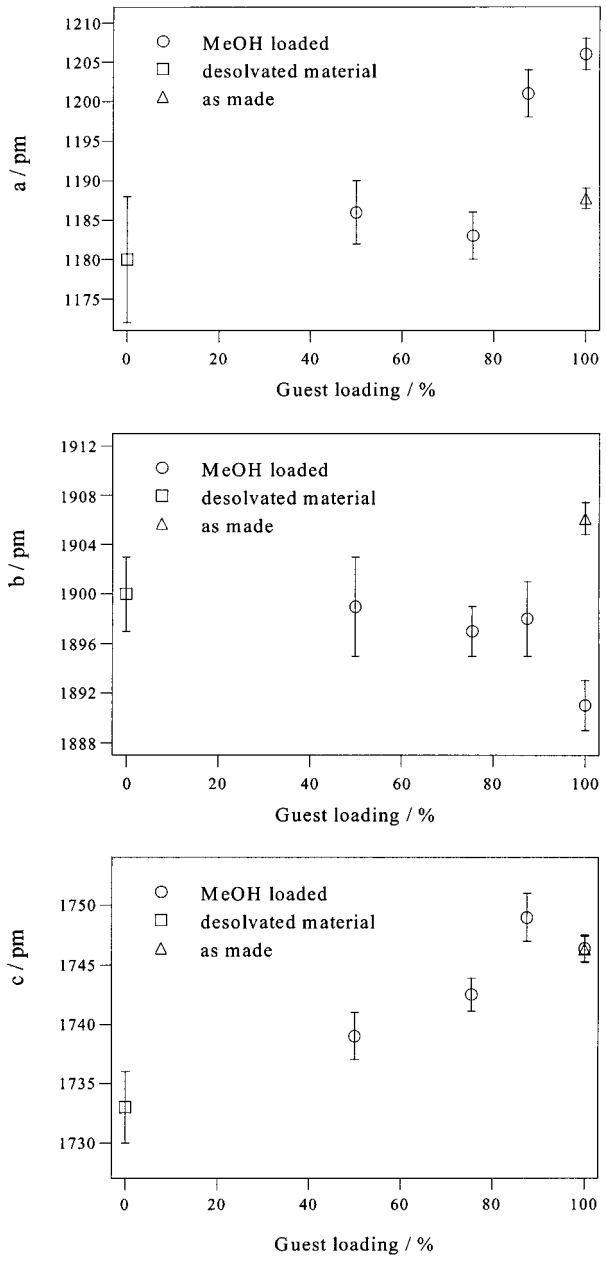

Figure 6. Variation in lattice parameters *a*, *b*, and *c* (top, middle, and bottom, respectively) for the Ni_2(4,4′-bipyridine)$_3(NO_3)_4$ host as a function of guest. The parameters for the as-made C_2H_5OH material are indicated by triangles; the desolvated material, by squares; and the various CH_3OH loadings, as circles.

$\ln(1 - M_t/M_e)$ versus time. Therefore, the uptake profiles for the uptake steps for both nitrous oxide and carbon dioxide do not follow either the LDF or CBRD models and may be described as biphasic, because an initial rapid uptake is observed.

X-ray Diffraction Measurements. The pore system of the parent phase, as determined by X-ray diffraction experiments, was evaluated using the Voids routine within the Ortex program.[39,40] This procedure divides the unit cell into cubic voxels (volume elements) of 80 pm side. If a given voxel lies more than 1.2 × (van der Waals radius) from the nearest atom, it is deemed to be a void and a "void atom" is inserted into this position. The resulting void atoms have been plotted in Figure 5. This approach reveals that the pore system is a unidirectional set of nonintersecting linear arrays of cavities with windows that connect cavities of ∼360 × 760 pm. The channels are predominantly lined by the π-systems of the 4,4′-bipyridine ligands and are not interconnected. The ethanol guests are located by hydrogen bonding to the nitrate group at well-defined sites (see Figure 5). The noncoordinating oxygen atom from each nitrate group is hydrogen bonded to the hydroxyl group of the guest. However, these hydroxyl positions are only 50% occupied in the as-prepared ethanol-templated material. The pore volume that is available controls the amount of methanol adsorbed, and steric considerations influence site occupation above adsorption of 2 methanol molecules. The volume occupied by the methanol molecule is ∼70% that of the ethanol molecule, and a stoichiometry of Ni_2(4,4′-bipyridine)$_3(NO_3)_4$·$3CH_3OH$ is expected. If all of the hydrogen bonding sites were to be occupied by methanol, the limiting composition would be Ni_2-(4,4′-bipyridine)$_3(NO_3)_4$·$4CH_3OH$.

(39) McArdle, P. *J. Appl. Crystallogr.* **1995**, *28*, 65.
(40) Burnett, M. N.; Johnson, C. K. *ORTEP III: Oak Ridge Thermal Ellipsoid Plot Program for Crystal Structure Illustrations*; Oak Ridge National Laboratory Report ORNL-6895; Oak Ridge National Laboratory: Oak Ridge, TN, 1996.

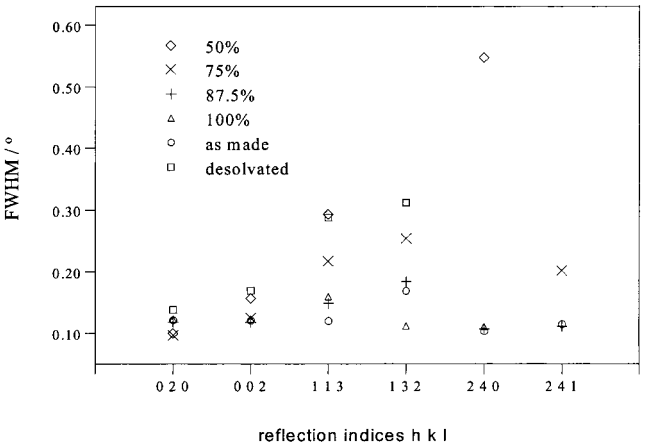

Figure 7. Variation in full-width at half-maximum (FWHM) as a function of guest loading in the $Ni_2(4,4'\text{-bipyridine})_3(NO_3)_4$ host for various reflections with various loadings of CH_3OH.

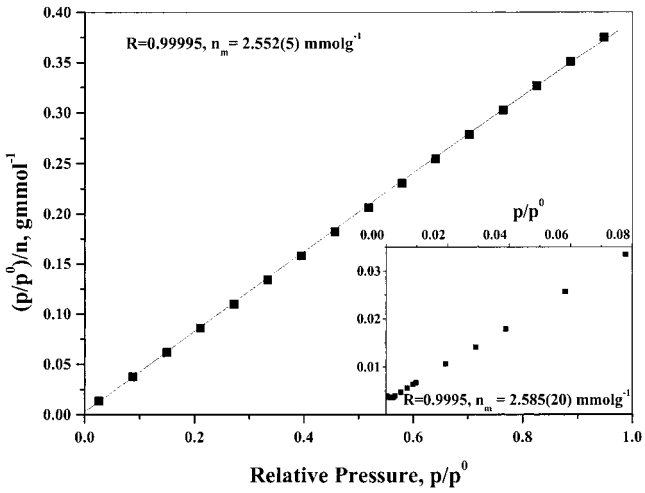

Figure 8. Langmuir isotherms for the adsorption of ethanol on $Ni_2(4,4'\text{-bipyridine})_3(NO_3)_4$ for pressure range $p/p^0 = 0-0.97$ ($p/p^0 = 0-0.08$, inset).

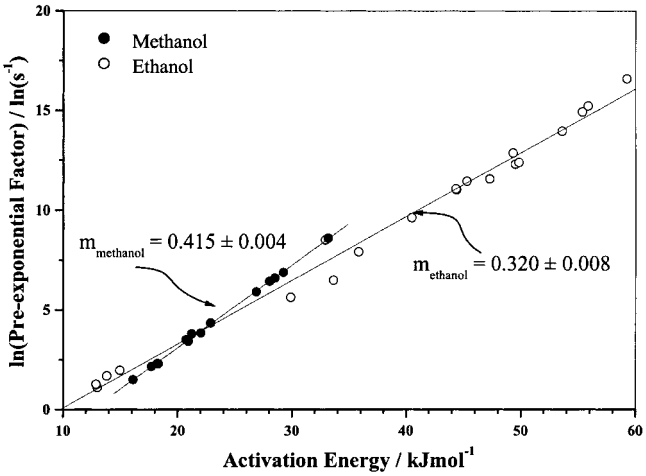

Figure 9. Variation of ln(preexponential factor) (ln(A)) with activation energy(E_a) for methanol(●) and ethanol(○).

X-ray powder diffraction showed that the 50% methanol-loaded sample is inhomogeneous but consists predominantly of the host structure. The 75% methanol-loaded material appeared to be a homogeneous single phase, but in the 100% loaded phase, some extra reflections attributable to the structure crystallized around methanol as a template were observed.[41] Two additional reflections in the range $20° < 2\theta < 25°$ were observed in the 87.5 and 100% samples. These could not be indexed using either of the known cells. However, these peaks could be indexed using a cell of the same dimensions as the ethanol cell but with no systematic absences present. It is, therefore, possible that these peaks are symptomatic of a reduction in symmetry at high methanol loadings. The absence of hysteresis in the adsorption isotherms indicates that none of these changes are irreversible.

The cell parameters for the methanol phase in each of the samples were extracted by fitting the peaks with a pseudo-Voigt peak shape and refining the lattice parameters using the LMGP suite of programs.[42] As shown in Figure 6, the cell volume increases on loading with methanol, the cell responding anisotropically to increased adsorbate (guest) concentration: the *a* cell parameter increases sharply, the *b* parameter decreases slightly, and *c* increases linearly within the precision of the data. The expansion of *a* is of particular interest, because this is the direction of the channels and suggests that the host is responding to the presence of the guest, in qualitative agreement with the steps seen in the sorption isotherms.

These diffraction data also contain information on the crystallinity of the sample. The data collected from both the evacuated material and the 50% methanol-loaded sample show considerable peak broadening and asymmetry in the case of the 50% loaded sample (see Figure 7). This suggests that the process of desolvation introduced disorder into the material on a length scale of ca. 100−500 Å. This loss of order will not necessarily reduce the sorption capacity of the material and appears to be reversible, as indicated by the absence of hysteresis in the sorption−desorption isotherms.

As the methanol loading is increased, the peaks show a reduction in width, indicating that a degree of recrystallization has occurred at high loadings. This observation, in addition to the presence of peaks due to the methanol-templated structure in the 100% loaded sample, shows that the adsorbent framework is capable of undergoing rearrangement in response to the introduction of methanol guest molecules. This rearrangement may be driven by increased ordering of the adsorbate (guest) molecules themselves and adsorbate/adsorbate (guest/guest) interactions as the adsorbate density in the channels increases and three methanol molecules are sorbed by hydrogen bonding per $Ni_2(4,4'\text{-bipyridine})_3(NO_3)_4$ unit. The occurrence of the isotherm step at the point where two methanol molecules are located in the channels, precisely matching the loading of hydrogen-bonding guests to that in the as-grown structure templated around ethanol, suggests that the structure itself is optimized for the uptake of two hydrogen-bonding guests and is forced to readjust upon the sorption of further guests. This demonstrates that in these flexible molecular frameworks, it is not simply the availability of void volume that controls guest uptake but the presence of a specific number of guest binding sites.

Discussion

Isotherm Analysis. Adsorption isotherms usually have a smooth continuous appearance, which is often a consequence of surface heterogeneity.[43] However, various types of adsorbate and adsorbent phase transformations may occur, but these are

(41) Cussen, E. J.; Claridge, J.; Rosseinsky, M. J. Unpublished results.

(42) Laugier, J.; Bochu, B. *LMGP - Suite of Programs for the Interpretation of X-ray Experiments*; ENSP/Laboratoire des Materiaux at du Genie Physique: Martin d'Heres, France, 2001.

(43) Adamson, A. W. *Physical Chemistry of Surfaces*, 5th ed.; Wiley: New York, 1990.

usually only visible on very uniform surfaces. A well-documented example of adsorbate structural change is the observation of steps in the nitrogen adsorption isotherm on a zeolite at 77 K, which has been attributed to a change in the density of the adsorbate with increased packing density at high relative pressure, consistent with that of a solid.[44] In Ni_2(4,4′-bipyridine)$_3$-$(NO_3)_4$, we have the possibility of both adsorbate- and adsorbent-phase transformations, and there is also the possibility of adsorbate/adsorbent interactions. In this study, the adsorption of carbon dioxide, nitrous oxide, nitrogen, and argon involve different interactions when compared with the hydrogen bonding to the nitrate in the case of methanol and ethanol adsorption on this functionalized flexible metal organic framework material.

Dubinin Radushkevich(D−R) Analysis. The adsorption characteristics of a range of adsorptives on microporous materials can be compared using the Dubinin−Radushkevich equation, which is as follows:

$$\log n = \log n_0 - D \log^2(p^0/p) \qquad (5)$$

where n is the amount adsorbed; n_0, the amount adsorbed corresponding to the micropore volume; p, the pressure; p^0, the saturated vapor pressure; and D is a constant related to the microporous structure of the adsorbent.[45] An estimate of the micropore volumes from nitrous oxide and carbon dioxide adsorption data both before and after the isotherm steps can be obtained using the D−R graphs. Extrapolation of the D−R graph for carbon dioxide for data below the isotherm step gave a lower micropore volume than the data after the step, whereas nitrous oxide adsorption shows the opposite trend. In the case of ethanol adsorption, in which cell expansion has been established unequivocally by X-ray diffraction studies,[22] extrapolation of the low-pressure data leads to an over-estimate of the micropore volume. Therefore, in this system, it is not possible to draw any firm conclusions regarding the nature of the structural change during the adsorption process from the D−R graphs.

Adsorption Dynamics. Rao et al. developed a model[46,47] for the interaction potential of diffusing species in porous carbons and concluded that two processes are involved in the adsorption dynamics: (a) diffusion along the pores, and (b) diffusion through the barrier at the pore entrance. A LDF model is followed when the latter is the rate-determining step, and a Fickian diffusion model is followed when the former controls the kinetics. When both processes are significant, a combined barrier resistance/diffusion model is followed. This has been observed for adsorption of a wide range of adsorptives on porous carbons.[28−34] At low loading, the adsorption kinetics follow a LDF model. The adsorbent structure changes during adsorption of ethanol, with two dimensions lengthening, the third shortening, and the space group remaining unchanged.[22] In the case of Ni_2(4,4′-bipyridine)$_3(NO_3)_4$, the pores are relatively large (360 × 720 pm) as compared with the barrier because of windows or entrances in the pore structure that control the diffusion into the porous material. These windows in the pore structure may be defined by the dimension between two oxygen atoms from nitrate groups and the dimension between two hydrogen atoms in the 2 position on the 4,4′-bipyridine ligands in an approximately perpendicular direction. In Ni_2(4,4′-bipyridine)$_3$-$(NO_3)_4$, the atom distances are O···O, 512 pm and H···H, 515 pm. Using van der Waals radii of 140 pm and 120 pm for the O and H atoms respectively, gives window dimensions of 232 pm (from O atoms) and 275 pm (from H atoms). The window is clearly too small for ethanol (416 × 427 × 633 pm) [48,49] to pass through without distorting the structure around the window. However, the crystal structure of the desolvated material, Ni_2-(4,4′-bipyridine)$_3(NO_3)_4$ has quite large displacement parameters for the nitrate and 4,4′-bipyridine (which rocks about the C_2 axis defined by the 1 and 4 positions on the ring). It is apparent that the pore structure undergoes structural change, allowing diffusion of guests into the pore structure, with host−guest interactions opening the windows in the pore structure and modifying adsorption characteristics.

At low surface coverage, the adsorption kinetics follow a LDF model. As the surface coverage increases, diffusion along the pores makes a significant contribution, and the CBRD model is obeyed for >50% loading for methanol and >90% loading for ethanol. Steric hindrance by the guests themselves for diffusion along the pores and the availability of specific adsorption sites are factors at high surface coverage. Previous studies of the diffusion of carbon dioxide into a carbon molecular sieve have shown that the mechanism can change from LDF through combined barrier resistance/diffusion to Fickian diffusion, with changes in adsorption temperature and pressure.[29] The rate constants obtained for methanol and ethanol adsorption are similar to those obtained for diffusion of gases and vapors into active carbons and carbon molecular sieves.[27−34] Eddaoudi et al. reported [4] the isotherm and kinetics for ethanol sorption on porous metal-organic framework material Zn_2(BTC)-$(NO_3)\cdot(C_2H_5OH)$, (BTC = 1,3,5-benzenetricarboxylate), for a single relative pressure (0.69 increment) at 295 K. The kinetics obtained from the $\ln(1 - M_t/M_e)$ versus time graph had three regions, with gradients corresponding to rate constants 5×10^{-5}, 3×10^{-3}, and 8×10^{-3} s^{-1}. It was proposed[4] that the kinetics were due to changes in zinc coordination number from 4 to 5 and 5 to 6 and pore filling in the final stage, respectively. The values of these rate constants are similar to those obtained for ethanol sorption on Ni_2(4,4′-bipyridine)$_3(NO_3)_4$.

The adsorption of ethanol on Ni_2(4,4′-bipyridine)$_3(NO_3)_4$ follows the Langmuir isotherm, which has the following form:

$$p/n = 1/n_m b + p/n_m \qquad (6)$$

where p is the pressure, n is the amount adsorbed, n_m is the monolayer capacity, and b is the coefficient of adsorption specific to the adsorbate/adsorbent system[1]. The Langmuir graph is dominated by the data for $p/p^0 > 0.075$, whereas 90% of the adsorption uptake occurs at $p/p^0 < 0.075$, as shown in Figure 8. The Langmuir graph for the relative pressure range (p/p^0) 0−0.08, which corresponds to >90% uptake ($R = 0.9995$) (see inset Figure 8), is not quite so good as the corresponding graph for p/p^0 0−0.97 ($R = 0.99995$). However, the graph is followed reasonably closely, bearing in mind the experimental errors associated with measuring adsorption isotherms at low (<0.2 mbar) vapor pressures. The exception is the very low-pressure region where a slight curvature is observed in the Langmuir graphs for all of the temperatures studied. It is apparent that

(44) Mueller, U.; Unger, K. K. In *Studies of Surface Science Catalysis*; Unger, K. K., Rouquerol, J., Sing, K. S. W., Kral, H. Eds. Elsevier: Amsterdam, 1987, Vol. 39, p 101.

(45) Dubinin, M. M. In *Characterization of Porous Solids*; Sing, K. S. W., Ed.; Society of Chemical Industries: London, 1979; Vol. 1, pp 1−11.

(46) Rao, M. B.; Jenkins, R. G.; Steele, W. A. *Ext. Abstr. Program − 17th Biennial Conference Carbon*; American Carbon Society: University of Kentucky, Lexington, 1985; p 114.

(47) Rao, M. B.; Jenkins, R. G.; Steele, W. A. *Langmuir* **1985**, *1*, 137.

(48) Webster, C. E.; Drago, R. S.; Zerner, M. C., *J. Am. Chem. Soc.* **1998**, *120*, 5509.

(49) Webster, C. E.; Zerner, M. C. Private communication calculated by the methods described in ref 48.

there is no evidence from either the isotherm or the Langmuir graph for a discrete change in the structure.

The Darken equation has been used to describe the variation of diffusivity (D) with surface coverage (θ), and in the case of a system obeying the Langmuir isotherm, the following relation has been derived.[50,51]

$$D_\theta/D_0 = 1/(1-\theta) \qquad (7)$$

where D_θ and D_0 are the diffusivities at θ and zero surface coverage, respectively. This implies that the diffusivities increase with increasing surface coverage. However, it is apparent from Figure 2 that the kinetic constants derived from the LDF model pass through a minimum. Further data are provided in Supporting Information. This indicates that for this material, which has a uniform pore size (360 × 720 pm) with barriers at the pore entrances and undergoes structural change during adsorption, the predictions of the Darken equation are not followed.

The adsorption kinetic data for methanol and ethanol, respectively, were used to calculate the barriers to diffusion into the porous material for changes in surface coverage. The results are shown Figure 2 ,and full details are given in Supporting Information. It is evident that the activation energies for ethanol adsorption are in general higher than those for methanol. A comparison of the adsorption rate constants with the activation energies for ethanol adsorption as a function of surface coverage shows that the minimum in the rate constant occurs at 50% total pore volume ($p/p^0 \sim 0.009$), and the maximum activation energy occurs at $p/p^0 \sim 0.0015$ (20% total pore volume). There is only a small change in activation energy up to 50% total pore volume, above which it decreases markedly. Methanol also shows a slight decrease in the rate constant with increasing p/p^0. However, a peak was observed in the activation energy graph at 44% total pore volume, but the peak is less clear, because the kinetic mechanism changes from LDF to the combined barrier resistance/diffusion model at 50% uptake, giving limited data above the peak. Ni_2(4,4′-bipyridine)$_3(NO_3)_4$ expands with increasing adsorption of both methanol and ethanol by a scissoring motion with the *a* and *c* crystallographic axes increasing and the *b* axis decreasing to accommodate more adsorbate. The X-ray data for 50% methanol uptake show a small increase in the *c* dimension, but the *a* and *b* dimensions are unchanged within experimental error. The 240 and 113 reflections also had a marked increase in peak width. This expansion is gradual, because the isotherms are smooth for both methanol and ethanol adsorption in the region of the peaks. It is apparent that the adsorption kinetics and barriers to diffusion are sensitive to relatively small changes in adsorbent structure.

Graphs of ln(preexponential factor) versus activation energy (E_a) for both methanol and ethanol adsorption on Ni_2(4,4′-bipyridine)$_3(NO_3)_4$ are linear, as shown in Figure 9. Graphs of ln(k) versus 1/T converge to well-defined isokinetic points with nonzero isokinetic rates for both methanol and ethanol adsorption. This is consistent with a true compensation effect.[52] Previous studies have shown that the adsorption of a wide range of adsorptives varying from water to *n*-nonane, thereby ranging from hydrophilic to hydrophobic character, on active carbon follow a compensation effect.[30,33,34] This was attributed to a mechanism in which a high barrier results in build-up of the adsorptive in front of the barrier, leading to an increased preexponential factor and vice versa.[33,34]

(50) Yang, R. T. *Gas Separation by Adsorption Processes*; Butterworths: Boston, **1987**.

(51) Kapoor, A.; Yang, R. T.; Wong, C. *Catal. Rev. Sci. Eng.* **1989**, *31*, 129.

(52) Agrawal, R. K. *J. Thermal Anal.* **1989**, *35*, 909.

Table 2. Comparison of the Molecular Dimensions (pm) Obtained from ZINDO Calculations for the Adsorptive Molecules Used in This Study[a]

adsorptive	dimensions/pm		
nitrogen	299.1	305.4	404.6
argon	351	364	
carbon dioxide	318.9	333.9	536.1
nitrous oxide[b]	303	304	532
methanol[b]	381	418	495
ethanol[b]	416	427	633

[a] Ref 48. [b] Ref 49.

The porous framework in Ni_2(4,4′-bipyridine)$_3(NO_3)_4$ is flexible, and the window in the porosity, which gives rise to the barriers to diffusion, changes in response to host−guest interactions. In these circumstances, in which the guest and pore sizes are similar, an estimate of guest size is of critical importance. There have been many different estimates of molecular dimensions.[48,53] Recently, an internally consistent set of molecular dimensions has been obtained[48,49] from zero integral neglect of differential overlap (ZINDO) methods, and these are given in Table 2. The adsorption of nitrous oxide and carbon dioxide are very fast, while methanol and ethanol have similar rate constants to those observed for kinetically selective adsorption situations with carbon molecular sieves.[28,29,31] Essentially, the rate constants for adsorption follow the trend expected from the minimum dimensions, that is, $C_2H_5OH < CH_3OH \ll CO_2$, N_2O. The activation energies for adsorption of ethanol (∼10−60 kJ mol^{-1}) are much higher than for methanol (16−33 kJ mol^{-1}) at the same loading, and this may be ascribed to the larger minimum dimensions of ethanol (416 × 427 pm), as compared with methanol (381 × 418 pm).[49]

Adsorption Thermodynamics. Hysteresis for the adsorption/desorption of methanol and ethanol on Ni_2(4,4′-bipyridine)$_3(NO_3)_4$ is insignificant in both cases. The isosteric enthalpies (ΔH_i) and entropies (ΔS_i) of adsorption were calculated at constant surface coverage using the following equation:

$$\ln(p) = \Delta H_i/RT - \Delta S_i/R \qquad (8)$$

where p is the pressure; R is the gas constant; and T (K), the temperature[1]. The values of ΔH_i and ΔS_i obtained for both methanol and ethanol adsorption on Ni_2(4,4′-bipyridine)$_3(NO_3)_4$ are similar to those obtained for the adsorption of ethanol and methanol on active carbons.[34]

The isosteric enthalpies of adsorption (ΔH_i) for ethanol, as shown in Figure 10, decreased gradually with increasing surface coverage. Ethanol adsorption gave values in the range 40−58 kJ mol^{-1}. The corresponding value for the heat of vaporization[36] is 38.6 kJ mol^{-1}. The ethanol guest-binding enthalpy, due predominantly to hydrogen bonding to the nitrate group, is effectively constant at low loading but then decreases at higher loading as a result of the expansion of the structure and by the destabilizing presence of other guests, presumably due to guest−guest or guest−host C−H repulsions as the channels become filled.

The values obtained for methanol adsorption were in the range of 39−56 kJ mol^{-1}, with a limiting isosteric enthalpy of ∼51 kJ mol^{-1} at zero surface coverage. This compares with the enthalpy of vaporization[36] of 35.2 kJ mol^{-1}. In the case of methanol, there is little change in ΔH_i, with surface coverage until the region of the isotherm step, as shown in Figure 10 when ΔH_i changes from ∼50 kJ mol^{-1} to 40 kJ mol^{-1}. ΔS_i changes from ∼ −200 to −160 J K^{-1} mol^{-1} in this region.

(53) Ainscough, A. N.; Dollimore, D. *Langmuir* **1987**, *3*, 708.

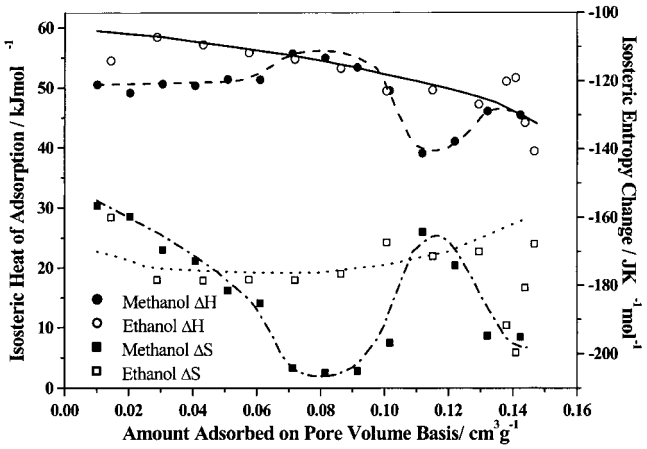

Figure 10. Thermodynamic data for the adsorption of methanol and ethanol on $Ni_2(4,4'\text{-bipyridine})_3(NO_3)_4$.

These changes in thermodynamic parameters are consistent with a change in the adsorbent structure and binding site rather than a change of the adsorbate from a liquid to a solidlike structure where a more ordered structure would be expected. This is entirely consistent with the powder diffraction observations. Furthermore, the likelihood of specific hydrogen bonding of the methanol molecules to the nitrate groups suggests a more solidlike adsorbed phase at lower relative pressures. The observation of the step at a methanol loading beyond one per metal center demonstrates that "overloading" of the binding capacity of a framework originally grown to accommodate one ethanol per metal, and directly correlates with the change in adsorption kinetics at this point.

Adsorption Kinetics and Thermodynamics in Relation to Structural Change. Nitrogen, carbon dioxide, and nitrous oxide have electrostatic moments that may interact with nitrate ions in the pore walls. However, this interaction will be much weaker than the interaction between alcohols and the nitrate. Grand Canonical Monte Carlo simulation studies have shown that the corners of rectangular nanopores act as sites for strong adsorption followed by multilayer formation or pore filling.[54] It is likely that the linear nitrogen, carbon dioxide, and nitrous oxide molecules fill the rectangular nanopores along the direction of the channel and interact more strongly with the π-system of the 4,4′-bipyridine units than the hydrogen-bonding nitrate units. It is energetically favorable for the carbon dioxide molecule to lie flat on the wall in order to make the three atoms of the molecule lie in the potential minimum.[55] Nitrogen also lies flat on the surface of graphite.[56] There is also the question of adsorbate packing in these rectangular pores. It is apparent from the steps in the adsorption isotherms presented in this paper that structural changes are induced at low relative pressures and surface coverage. This may be due to the critical influence of adsorption in the corners of the pores, which induces structural relaxation. It is proposed that small structural changes resulting from adsorption at the corners may be magnified in the more flexible parts of the porous framework material, resulting in more pronounced structural changes and steps in the isotherms.

In the case of ethanol adsorption, the isotherms follow the Langmuir model very closely. ΔH_i and ΔS_i do not change markedly with increasing surface coverage until $p/p^0 = 0.34$ (~95% pore volume) and are similar to those observed for the adsorption of ethanol on active carbons.[34] The rate constants decrease with increasing relative pressure reaching a minimum at $p/p^0 = \sim 0.009$ (~50% pore volume) and increase thereafter up to >90% pore filling before the kinetic model changes from linear driving force to a combined barrier resistance/diffusion model. A linear driving force model indicates that diffusion through barriers in the pore structure is the rate-determining step, but a combined barrier resistance/diffusion model indicates the importance of both diffusion through barriers and along pores. The increasing importance of diffusion along the pores at high surface coverage is expected because of the decreasing availability of specific adsorption sites. The activation energies for diffusion of ethanol into the porous structure increase with increasing relative pressure reaching a maximum at $p/p^0 = 0.0015$ (20% pore volume). However, there is only a very small change in activation energy up to 50% pore volume, after which there is a marked decrease. This suggests that the structure starts to relax significantly at ~50% pore volume with the scissoring motion shown by the X-ray structure determinations[22] of $Ni_2(4,4'\text{-bipyridine})_3(NO_3)_4$ and $Ni_2(4,4'\text{-bipyridine})_3(NO_3)_4 \cdot 2C_2H_5OH$. This latter structure indicates that the ethanol molecules are localized by hydrogen bonding to the nitrate with four nitrate ions surrounding two ethanol molecules. However, there is disorder in the unidentate and bidentate nitrate ions. This may be a factor in the marked change in activation energy at 50% pore volume. The coordination of the ethanol molecules to the nitrate ions indicates that the adsorbed ethanol is more solidlike rather than liquidlike. A comparison of the two structures indicates the window in the pore structure composed of nitrate and 4,4′-bipyridine ligands changes, and this flexibility influences diffusion into the porous structure.

The total pore volumes obtained from the ethanol and methanol adsorption isotherms were similar. However, the methanol adsorption isotherm is quite different and has a step at ~70% pore volume that corresponds to sorption of two molecules of methanol per dimer unit. It is proposed that this step is indicative of a structural rearrangement of the host structure to allow methanol adsorption on sites that are in addition to those sites occupied in the material fully loaded with ethanol. There is qualitative support for this argument in the X-ray powder diffraction data collected from the material at various methanol loadings. These data show that the process of evacuation leads to a reduction in the crystallinity of the framework structure and that this disorder is present in the 50% methanol loaded sample. However, for loadings of >75%, a reduction in the peak widths is observed, indicating that the long-range order of the host structure is increasing. This suggests that in order for the methanol loading level to increase beyond $Ni_2(4,4'\text{-bipyridine})_3(NO_3)_4 \cdot 2CH_3OH$, the framework structure needs to change subtly. The changes in the lattice parameters with methanol loading do not show a clear step at 75% loading, but a small change in the ordering of the host structure (e.g., rocking of the aromatic rings of the 4,4′-bipyridine ligands or movement of the nonbinding oxygen atoms of the nitrate group) would be beyond the detection limits of the X-ray powder diffraction data. This would, instead, require a careful single crystal study, a requirement that is incompatible with the isotherm experiments. The *a* dimension increases quite markedly, with further increase in methanol adsorption above 75% loading, and this is accompanied by a decrease in the *b* dimension and further increase in the *c* dimension. The X-ray diffraction data show that the host structure is responding in a nonlinear way to methanol adsorption, in agreement with the isotherm measurements.

(54) Bojan, M.; Steele, W. A. *Carbon* **1998**, *36*, 1417.
(55) Vishnyakov, A.; Ravikovitch, P. I.; Neimark, A. V. *Langmuir* **1999**, *15*, 8736.
(56) Steele, W. A. *Chem. Rev.* **1993**, *93*, 2355.

The methanol adsorption isotherms give values for ΔH_i that do not change markedly, although ΔS_i initially becomes more negative with increasing surface coverage up to ~60% methanol loading. Thereafter, ΔH_i decreases and ΔS_i becomes more positive up to ~70% loading (pore volume ~ 0.11 cm^3g^{-1}) in which the step in the isotherm is observed. The adsorption kinetics slow when the step occurs. This agrees with our model of methanol initially filling the sites occupied by ethanol. The changes in adsorption thermodynamic and kinetic parameters are presumably related to the structural change. At higher loadings, ΔH_i increases and ΔS_i becomes more negative as the different types of adsorption sites are occupied. Presumably, this involves adsorption on the more hydrophobic π-systems of the 4,4′-bipyridine ligands.

Conclusions

The adsorption isotherms of gases and vapors on $Ni_2(4,4'\text{-bipyridine})_3(NO_3)_4$ are surprisingly complex, with steps in the isotherms that vary with the adsorptive and temperature. Carbon dioxide and nitrous oxide have very similar isotherms, with steps in the isotherm at low surface coverage associated with a marked slowing in the adsorption kinetics. At low relative pressure, adsorption is likely to occur on the aromatic parts of the porous framework material, in particular, in the corners of the rectangular pores. It is proposed that adsorption in the corners of rectangular pores is critical in inducing structural change by flexible parts of the host adsorbent.

Ethanol adsorption results in the $Ni_2(4,4'\text{-bipyridine})_3(NO_3)_4$ structure undergoing a scissoring movement, with two cell dimensions increasing and the third decreasing, but the unit cell space group remains unchanged. However, ethanol adsorption follows a Langmuir isotherm over the temperature range studied. Methanol adsorption isotherms have steps that are observed at high surface coverage and are associated with a marked slowing in the adsorption kinetics. The origin of the isotherm steps is most likely due to adsorbent structural change in order to allow adsorption on different surface sites after complete occupation of the nitrate sites. Thermodynamic data for methanol adsorption in the region of the isotherm step supports this conclusion. The porous framework is flexible and host−guest interactions modify the windows/pore entrances in the porosity, which form the barrier to diffusion of the adsorptive into the porous structure. The activation energies for adsorption of ethanol (10−60 kJ mol^{-1}) are much higher than for methanol (16−33 kJ mol^{-1}) at the same surface coverage. This can be attributed to the small differences in the size of the adsorptives. The observation that the activation energies for both methanol and ethanol go through a maximum is consistent with structural relaxation to accommodate more adsorbate. However, in the case of ethanol, no isotherm step was observed, and the methanol isotherm step was observed at higher surface coverage than the peak in the activation energy. This indicates that cell expansion is not necessarily linked to steps in the isotherm.

Acknowledgment. The authors thank Dr. C. E. Webster of Texas A&M University and the late Dr. M. C. Zerner of Florida State University for providing additional calculations of the adsorptive dimensions for methanol, ethanol, and nitrous oxide.

Supporting Information Available: Adsorption isotherm and kinetic data are available free of charge via the Internet at http://pubs.acs.org.

JA0109895